Nonisolated ZVZCS Resonant PWM DC–DC Converter for High Step-Up and High-Power Applications

Yohan Park, Byoungkil Jung, and Sewan Choi, *Senior Member, IEEE*

***Abstract*—The demand for nonisolated high step-up dc–dc converters in applications such as dc backup energy systems for UPS, photovoltaic and fuel cell systems, and hybrid electric vehicles has been gradually increasing. This paper proposes nonisolated step-up dc–dc converters with an improved switching method. The proposed converter shows zero-voltage switching turn-on of the switches in continuous conduction mode as well as reduced turn-off switching losses owing to the switching method that utilizes L_r–C_r resonance in the auxiliary circuit. Also, as a result of the proposed switching method, the switching losses associated with diode reverse recovery become negligible even in the small duty cycle. The capacitance in the auxiliary circuit is significantly reduced compared to the pulsewidth modulation method. The duty cycle loss is further reduced resulting in increased step-up ratio. Experimental results from a 2-kW prototype of a two-phase interleaved version are also provided to validate the proposed concept.**

***Index Terms*—High step-up, high-voltage gain, nonisolated, soft-switched.**

I. Introduction

THE demand for nonisolated high step-up dc–dc converters has been gradually increasing in accordance with the growth in dc backup energy systems for uninterruptible power system (UPS), photovoltaic systems, fuel cell systems, and hybrid electric vehicles. Since the general boost converter should operate at high duty cycle in order to achieve high-output voltage, the rectifier diode must sustain a short pulse current with high amplitude, resulting in severe reverse recovery as well as high electromagnetic interference problems. Also, as output voltage is increased, the switch voltage rating is increased, which increases the dominating conduction loss. Moreover, a high duty cycle may lead to poor dynamic responses to line and load variations.

Manuscript received December 9, 2011; accepted January 25, 2012. Date of current version April 20, 2012. This work was supported in part by Seoul National University of Science and Technology and by a National Research Foundation of Korea (NRF) grant funded by the Korea Government (MEST) (No. 2011-0018025). Recommended for publication by Associate Editor S. D. Pekarek.

Y. Park is with LG Electronics Company, Ltd., Seoul 153-802, Korea (e-mail: john99.park@lge.com).

B. Jung and S. Choi are with the Department of Control and Instrumentation Engineering, Seoul National University of Science and Technology, Seoul 139-743, Korea (e-mail: jbk0917@nate.com; schoi@seoultech.ac.kr).

Color versions of one or more of the figures in this paper are available online at http://ieeexplore.ieee.org.

Digital Object Identifier 10.1109/TPEL.2012.2187342

Various types of nonisolated high step-up dc–dc converters have been presented to overcome the aforementioned problem. Converters with coupled inductors [1]–[5] can provide high-output voltage without using high duty cycle and yet reduce the switch-voltage stress. The reverse recovery problem associated with rectifier diode is also alleviated. However, they have large input current ripple and are not suitable for high-power applications since the capacity of the magnetic core is considerable. The switched-capacitor converter [6]–[10] does not employ an inductor making it feasible to achieve high-power density. However, the efficiency could be reduced to allow output voltage regulation. The major drawback of theses topologies is that attainable voltage gains and power levels without degrading system performances are restricted.

Most of the coupled-inductor and switched-capacitor converters are hard-switched and, therefore, they are not suitable for high efficiency and high-power applications. Some soft-switched interleaved high step-up converter topologies [11]–[18] have been proposed to achieve high efficiency at desired level of volume and power level. Among them, the soft-switched continuous conduction mode (CCM) boost converter [14] demonstrated reduced voltage stresses of switches and diodes and zero-voltage switching (ZVS) turn-on of the switches in CCM and zero-current switching (ZCS) turn-off of the diodes. However, a drawback of this pulsewidth modulation (PWM) converter is high turn-off switch losses.

In this paper, an improved switching method, called resonant PWM (RPWM) is proposed for the soft-switched CCM boost converter in order to reduce the turn-off switching losses. Since the RPWM is performed by utilizing L_r–C_r resonance in the auxiliary circuit, the capacitance is significantly reduced. Also, because of the proposed RPWM operation, the switching losses associated with diode reverse recovery become negligible even in the small duty cycle and the duty cycle loss is further reduced resulting in increased step-up ratio. The operating principles along with a design example of the proposed converter are described. Experimental results from a 2-kW prototype of a two-phase interleaved version are also provided to validate the proposed concept.

II. Operating Principles of the Proposed Converter

Fig. 1 shows the circuit diagram of the proposed converter which has the same circuit topology as the PWM method proposed in [14]. The proposed converter consists of a general boost converter as the main circuit and an auxiliary circuit which

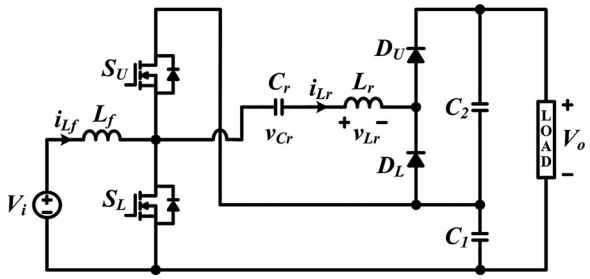

Fig. 1. Proposed ZVZCS RPWM dc–dc converter.

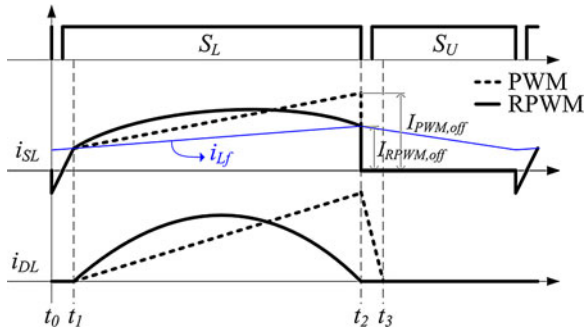

Fig. 2. Comparison of switch and diode current waveforms of two methods (C_r variation).

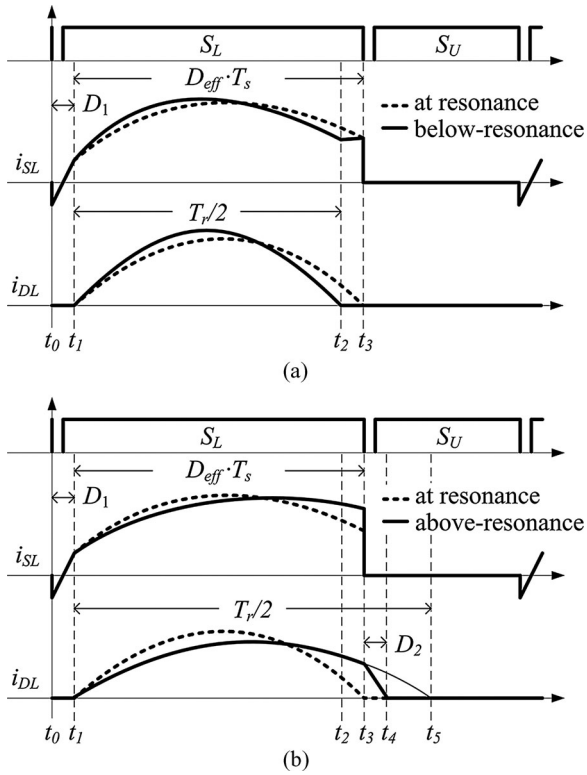

Fig. 3. Comparison of switch and diode current waveforms of two resonance operations (f_r variation). (a) Below-resonance operation ($T_r < 2D_{\rm eff}T_s$). (b) Above-resonance operation ($T_r > 2D_{\rm eff}T_s$).

includes capacitor C_r, inductor L_r, and two diodes D_L and D_U. Two switches are operated with asymmetrical complementary switching to regulate the output voltage. Owing to the auxiliary circuit, not only output voltage is raised but ZVS turn-on of two switches can naturally be achieved in CCM by using energy stored in filter inductor L_f and auxiliary inductor L_r. Unlike PWM method [14] in which the switches are turned OFF with high peak current, the proposed converter utilizes L_r–C_r resonance of auxiliary circuit, thereby reducing the turn-off current of switches. Furthermore, for resonance operation, the capacitance of C_r is reduced by at least 20-fold, resulting in reduced volume. Also, switching losses associated with diode-reverse recovery of the proposed RPWM converter are significantly reduced.

A. PWM Method Versus RPWM Method

Fig. 2 shows the current waveforms of lower switch S_L and lower diode D_L of the converter illustrating the effectiveness of the proposed RPWM. As shown in Fig. 2, $I_{\rm RPWM,off}$, switch turn-off current of the proposed RPWM method, is smaller than $I_{\rm PWM,off}$, switch turn-off current of PWM method which is the sum of input inductor current i_{Lf} and auxiliary inductor current i_{Lr} at turn off instant. In fact, $I_{\rm RPWM,off}$ is the same as the turn-off current of the general boost converter. For the proposed RPWM operation, resonant capacitor C_r is reduced by at least 20-fold compared to the auxiliary capacitor of the PWM operation which should be large enough to act as a voltage source. Furthermore, the turn-off losses associated with diode reverse recovery of the proposed RPWM converter are negligible while that of the PWM method could be somewhat considerable, especially at operation with small duty, due to high turn-off current and di/dt, as shown in Fig. 2.

B. Above-Resonance Operation Versus Below-Resonance Operation

Fig. 3 shows the two resonance operations according to the variations of resonant frequency $f_r(1/T_r)$ which is expressed as in (1): the below-resonance operation ($2f_r > f_s/D_{\rm eff}$), and the above-resonance operation ($2f_r < f_s/D_{\rm eff}$)

$$f_r = \frac{1}{2\pi\sqrt{L_r C_r}}. \tag{1}$$

It can be seen from Fig. 3 that the below-resonance operation has advantages over the above-resonance operation. First, the total switching losses are smaller for the below-resonance operation since both switch turn-off current and diode di/dt are smaller. Second, duty loss D_1 of the below-resonance operation is smaller than duty loss D_1+D_2 of the above-resonance operation, as shown in Fig. 3. The below-resonance operation is chosen for the proposed RPWM method. For below-resonance operation, half of the resonant period (t_1–t_2) should be shorter than $D_{\rm eff}T_s(t_1$–$t_3)$. Therefore, the resonant frequency can be determined by

$$f_r > \frac{f_s}{2D_{\rm eff}} \tag{2}$$

where $D_{\rm eff}$ is effective duty cycle D–D_1 considering the duty loss.

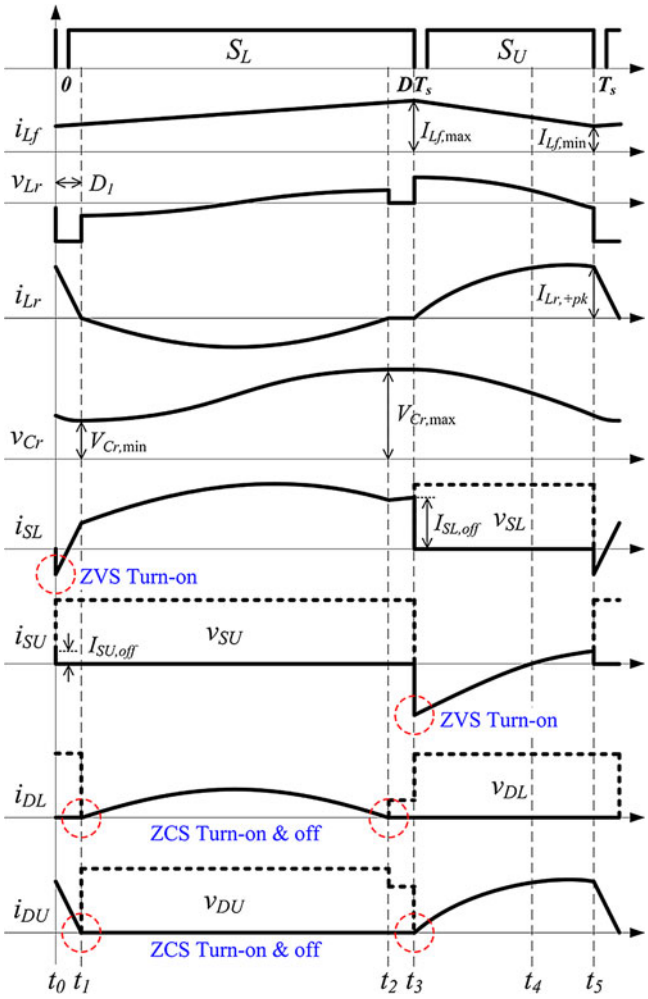

Fig. 4. Key waveforms of the proposed RPWM converter.

C. Operating Modes

The operating modes and key waveforms of the proposed converter are shown in Figs. 4 and 5. In the below-resonance operation, five modes exist within T_s.

Mode 1 (t_0 – t_1): This mode begins when upper switch S_U which was carrying the current of difference between i_{Lf} and i_{Lr} is turned OFF. S_L can be turned ON with ZVS if gate signal for S_L is applied before the current direction of S_L is reversed. Filter inductor current i_{Lf} and auxiliary current i_{Lr} starts to linearly increase and decrease, respectively, as follows

$$i_{Lf}(t) = \frac{V_i}{L_f}(t - t_0) + i_{Lf}(t_0) \tag{3}$$

$$i_{Lr}(t) = \frac{V_{Cr,\min} - V_o}{L_r}(t - t_0) + i_{Lr}(t_0). \tag{4}$$

This mode ends when decreasing current i_{Lr} changes its direction of flow. Then D_U is turned OFF under ZCS condition.

Mode 2 (t_1–t_2): This mode begins with L_r–C_r resonance of the auxiliary circuit. Fig. 6(a) shows equivalent circuit of this resonant mode. Current i_{Lf} is still linearly increasing. The voltage and current of resonant components are determined, respectively, as follows:

$$i_{Lr}(t) = -i_{Cr}(t) = \frac{V_{r,2}}{Z}\sin(\omega_r(t - t_1)) \tag{5}$$

$$v_{Cr}(t) = V_{r,2}[\cos(\omega_r(t - t_1)) - 1] + v_{Cr}(t_1) \tag{6}$$

where $V_{r,2} = V_{Cr,\min} - V_{C1}$, $Z = \sqrt{L_r/C_r}$, and $\omega_r = 1/\sqrt{L_r C_r}$. This resonance mode ends when i_{Lr} reaches to zero. Note that D_L is turned OFF under ZCS condition.

Mode 3 (t_2–t_3): There is no current path through the auxiliary circuit during this mode. Output capacitors supply the load. At the end of this mode the turn-off signal of S_L is applied. It is noted that the turn-off current of S_L, $I_{\mathrm{SL,off}}$ is limited to filter inductor current at t_3, $I_{Lf,\max}$, which is much smaller than that of PWM method.

Mode 4 (t_3–t_4): This mode begins when lower switch S_L is turned OFF. S_U can be turned ON with ZVS if gate signal for S_U is applied before the current direction of S_U is reversed. Filter inductor current i_{Lf} starts to linearly decrease since voltage v_{Lf} becomes negative

$$i_{Lf}(t) = \frac{V_i - V_{C1}}{L_f}(t - t_3) + i_{Lf}(t_3). \tag{7}$$

Like Mode 2, the other L_r–C_r resonance of auxiliary circuit is started, and D_U starts conducting. Equivalent circuit of resonant mode is shown in Fig. 6(b). The voltage and current of resonant components are determined, respectively, as follows:

$$i_{Lr}(t) = -i_{Cr}(t) = \frac{V_{r,4}}{Z}\sin(\omega_r(t - t_3)) \tag{8}$$

$$v_{Cr}(t) = V_{r,4}[\cos(\omega_r(t - t_3)) - 1] + v_{Cr}(t_3) \tag{9}$$

where $V_{r,4} = V_{Cr,\max} - V_{C2}$, $Z = \sqrt{L_r/C_r}$, and $\omega_r = 1/\sqrt{L_r C_r}$.

This mode ends when i_{Lr} is equal to i_{Lf}.

Mode 5 (t_4–t_5): After i_{Lr} equals i_{Lf}, i_{SU} changes its direction, then this mode begins. At the end of this mode, turn-off signal of S_U is applied and this mode ends.

D. Voltage Conversion Ratio

To obtain the voltage gain of the proposed converter, it is assumed that the voltage across C_1 and C_2 are constant during the switching period T_s. The output voltage is given by

$$V_o = V_{C1} + V_{C2}. \tag{10}$$

It can also be expressed as

$$V_o = \frac{2}{1 - D_{\mathrm{eff}}}V_i = \frac{2}{1 - D}V_i - \Delta V \tag{11}$$

where effective duty D_{eff} and voltage drop ΔV are expressed using duty loss ΔD

$$D_{\mathrm{eff}} = D - \Delta D \tag{12}$$

$$\Delta V = \frac{2\Delta D V_i}{(1 - D)(1 - D_{\mathrm{eff}})}. \tag{13}$$

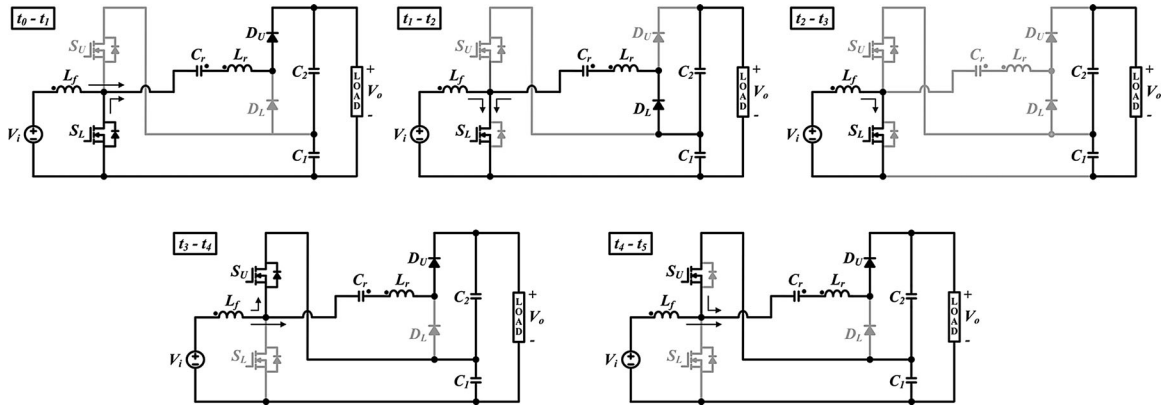

Fig. 5. Operating modes of the proposed RPWM converter.

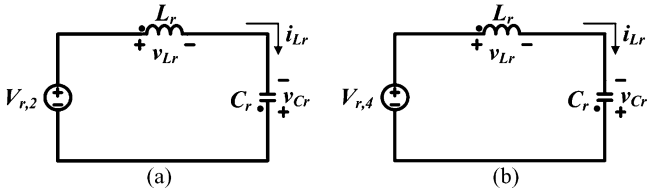

Fig. 6. Equivalent circuit of resonant mode. (a) Mode 2 (t_1–t_2). (b) Mode 4–5 (t_3–t_5).

V_{C1} that is the same as output voltage of the general boost converter can be expressed as

$$V_{C1} = \frac{1}{1-D} \cdot V_i. \tag{14}$$

From (10), (11), and (14), V_{C2} can be expressed as

$$V_{C2} = \frac{1}{1-D} V_i - \Delta V. \tag{15}$$

In the steady state, the average load current equals the average current of diodes D_L and D_U. Since i_{Lr} flows through the D_L during mode 2, the average load current can be obtained as follows:

$$I_{\mathrm{DL,av}} = \frac{V_o}{R_o} = \left| \frac{2}{T_s} \int_0^{T_r/4} (V_{Cr,\min} - V_{C1}) \frac{\sqrt{C_r}}{\sqrt{L_r}} \sin(\omega_r t) \cdot dt \right| \tag{16}$$

From (16), $V_{Cr,\min}$ and $V_{Cr,\max}$ of capacitor voltage V_{Cr} can be approximated by

$$V_{Cr,\min} \approx V_{C1} - \frac{V_o}{2C_r R_o f_s} \tag{17}$$

$$V_{Cr,\max} \approx V_{C1} + \frac{V_o}{2C_r R_o f_s}. \tag{18}$$

1) *Below-resonance operation* ($D > f_s/2f_r$)*:*
In this mode, the duty loss is the same as D_1, as shown in Fig. 7(a). The steady-state inductor voltage equation on inductor L_r during $D_1 T_s$ gives

$$V_{Cr,\min} - V_o = L_r \frac{\sqrt{C_r/L_r}(V_{Cr,\max} - V_{C2})}{D_1 T_s}. \tag{19}$$

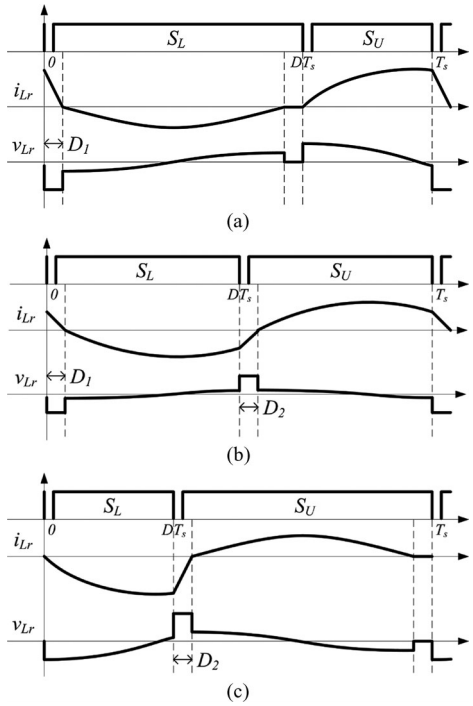

Fig. 7. Three modes according to operating duty ratio. (a) Below-resonance operation with $D > f_s/2f_r$. (b) Above-resonance operation with $1-(f_s/2f_r) < D < f_s/2f_r$. (c) Above-resonance operation with $D < 1-(f_s/2f_r)$.

From (17), (18), and (19), the duty loss can be obtained by

$$\Delta D = D_1 = \frac{(1-D)(f_s/\omega_r)\sin((1-D)\omega_r/f_s)}{2C_r R_o f_s (V_i/V_o) + (1-D)}. \tag{20}$$

From (11) and (20), the voltage gain in this mode can be obtained by

$$M = \frac{D'(1-A) + \sqrt{[D'(A-1)]^2 + 4AD'(D'+B)}}{D'(D'+B)} \tag{21}$$

where

$$D' = 1 - D,\ A = C_r R_o f_s, \text{ and } B = \left(\frac{f_s}{\omega_r}\right) \sin\left(\frac{D'\omega_r}{f_s}\right).$$

2) *Above-resonance operation* $(1 - (f_s/2f_r) < D < (f_s/2f_r))$:
In this mode, the duty loss is $D_1 + D_2$ as shown in Fig. 7(b). In a similar way, the duty loss can be obtained as follows:

$$\Delta D = D_1 + D_2 = \frac{2(1-D)(f_s/\omega_r)\sin(\omega_r/2f_s)\cos((D-0.5)\omega_r/f_s)}{2C_r R_o f_s (V_i/V_o) + (1-D)} \tag{22}$$

From (11) and (22), the voltage gain of this mode can be obtained by

$$M = \frac{D'(1-A) + \sqrt{[D'(A-1)]^2 + 4AD'(D'+C)}}{D'(D'+C)} \tag{23}$$

where

$$C = 2\frac{f_s}{\omega_r}\sin\left(\frac{\omega_r}{2f_s}\right)\cos\left(\frac{(D-0.5)\omega_r}{f_s}\right).$$

3) *Above-resonance operation* $(D < 1 - (f_s/2f_r))$:
In this mode, the duty loss is D_2, as shown in Fig. 7(c). In a similar way, the duty loss can be obtained as follows:

$$\Delta D = D_2 = \frac{(1-D)(f_s/\omega_r)\sin(D\omega_r/f_s)}{2C_r R_o f_s (V_i/V_o) + (1-D)}. \tag{24}$$

From (11) and (24), the voltage gain of this mode can be obtained by

$$M = \frac{D'(1-A) + \sqrt{[D'(A-1)]^2 + 4AD'(D'+E)}}{D'(D'+E)} \tag{25}$$

where

$$E = \frac{f_s}{\omega_r}\sin\left(\frac{D\omega_r}{f_s}\right).$$

From (21), (23), and (25), the voltage gain of the converter using the proposed RPWM method is drawn in Fig. 8 as a function of duty ratio D. Compared to the PWM method proposed in [14], the voltage gain of the proposed RPWM is increased by 10–30% according to operating duty.

E. ZVS Characteristic for Switches

As shown in Fig. 4, ZVS of the lower switch is achieved when the upper switch is turned OFF at t_0. The ZVS current of lower switch $I_{\mathrm{SL,ZVS}}$ is determined by the difference between i_{Lf} and i_{Lr} at t_0, as follows:

$$I_{\mathrm{SL,ZVS}} = I_{Lr,+pk} - I_{Lf,\min} = \frac{L_f\left[V_i I_o \omega_r T_s \sin(\omega_r(1-D)T_s) - 2P_o\right] + DT_s V_i^2}{2V_i L_f}. \tag{26}$$

The ZVS of the upper switch is achieved when the lower switch is turned OFF at t_3. The ZVS current of upper switch

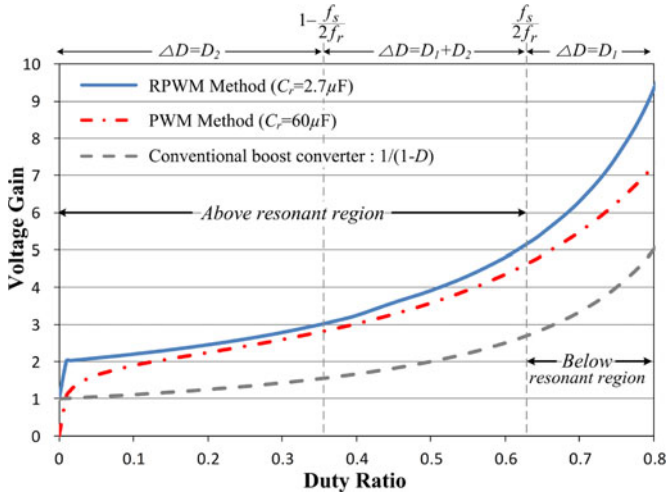

Fig. 8. Voltage gain of the proposed converter ($V_i = 70$ V, $L_r = 6$ μH, $f_s = 50$ kHz, and $R_o = 72\ \Omega$).

$I_{\mathrm{SU,ZVS}}$ is the peak of i_{Lf}, as follows:

$$I_{\mathrm{SU,ZVS}} = I_{Lf,\max} = \frac{2P_o L_f + DT_s V_i^2}{2V_i L_f}. \tag{27}$$

To ensure ZVS turn-on of lower switch S_L, the following condition should be satisfied:

$$\frac{1}{2}L_r(I_{Lr,+pk} - I_{Lf,\min})^2 > \frac{1}{2}(C_{\mathrm{OS},L} + C_{\mathrm{OS},U})\left(\frac{V_i}{1-D}\right)^2 \tag{28}$$

where $C_{\mathrm{OS},L}$ and $C_{\mathrm{OS},U}$ are the output capacitance of lower and upper switches, respectively.

To ensure ZVS turn-on of upper switch S_U, the following condition should be satisfied:

$$\frac{1}{2}L_f I_{Lf,\max}^2 > \frac{1}{2}(C_{\mathrm{OS},L} + C_{\mathrm{OS},U})\left(\frac{V_i}{1-D}\right)^2. \tag{29}$$

In fact, the condition of (29) can easily be satisfied, and therefore, ZVS of upper switch can be achieved over the whole load range. On the other hand, the condition of (28) may not be satisfied under the conditions of small auxiliary inductor L_r and/or large filter inductor L_f.

Using (26)–(29), the ZVS currents and ZVS ranges of lower and upper switches as the function of output power and input voltage are plotted, respectively, as shown in Fig. 9. As shown in Fig. 9(a), the ZVS current of the lower switch tends to decrease as the output power increases. This means that the ZVS turn-on of the lower switch can be more easily achieved under the condition of smaller output power. The ZVS range of the lower switch becomes broader for smaller total output capacitance $C_{\mathrm{OS,tot}} = C_{\mathrm{OS},L} + C_{\mathrm{OS},U}$ of MOSFETs. On the other hand, the ZVS current of the upper switch tends to increase as the output power increases. It should be noted from Fig. 9(b) that the ZVS turn-on of the upper switch can be achieved in the overall output power and input voltage.

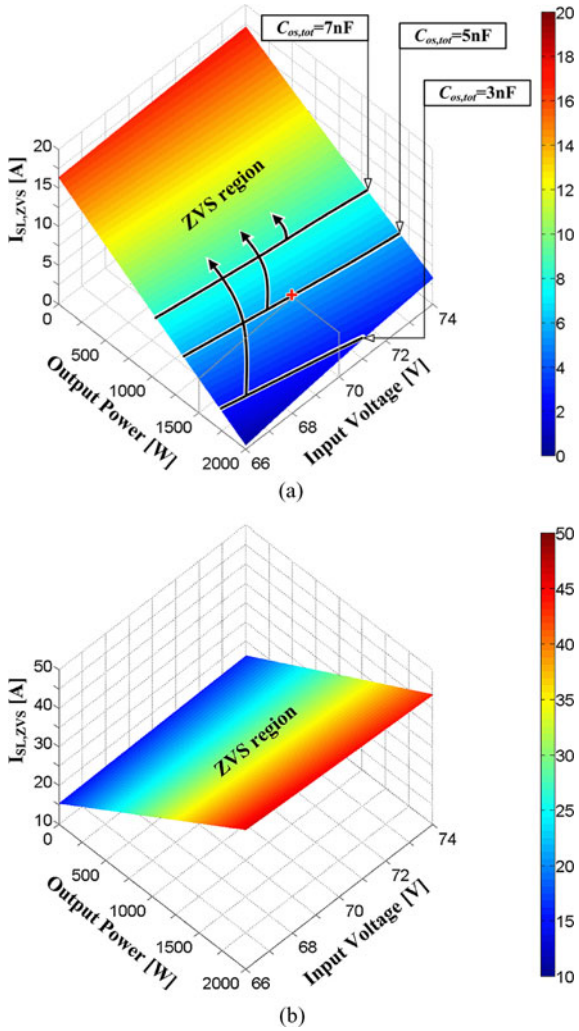

Fig. 9. ZVS currents and ZVS ranges of lower and upper switches as the function of the output power and input voltage. (a) Lower switches. (b) Upper switches (V_o = 380 V, P_o:100 W–2 kW, L_r = 6 μH, C_r = 2.7 μF, and f_s = 50 kHz).

III. Design of the Proposed Converter

The generalized scheme of the proposed converter has been shown in [15], where it is configured with proper numbers of series and parallel connected basic cells. This leads to flexibility in device selection resulting in high-component availability and easy thermal distribution. A specification for a design example in this paper is given as follows and the chosen circuit topology for the specification is shown in Fig. 10

$$P_o = 2\,\text{kW},\quad V_o = 380\,\text{V},\quad V_i = 70\,\text{V}$$
$$f_s = 50\,\text{kHz},\ \Delta I_{\text{in}} = 30\%,\ \Delta V_o = 5\%.$$

A. Design of L_f

Considering input current ripple ΔI_{in}, input inductor L_f is determined by

$$L_f = \frac{1}{2}\cdot\frac{D\cdot V_{\text{in}}}{\Delta I_{\text{in}}\cdot f_s} = 50\ \mu\text{H}. \tag{30}$$

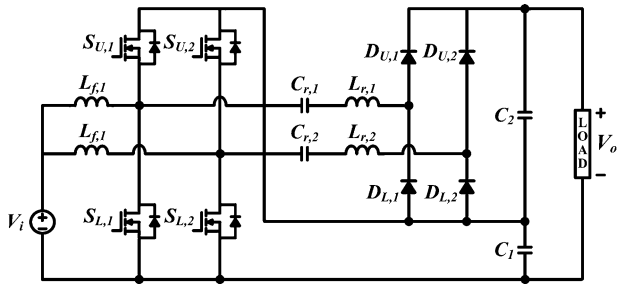

Fig. 10. Circuit diagram of the proposed converter with $N = 1$ and $P = 2$.

TABLE I
COMPARISON OF PERFORMANCE OF THE PROPOSED RPWM METHOD AND THE PWM METHOD (P_o = 2 kW, V_i = 70 V, V_o = 380 V, f_s = 50 kHz, N = 1, AND P = 2)

		PWM Method in [14]	Proposed RPWM Method
Operating duty cycle		0.648	0.638
Switches	V_{pk}	4×199V	4×193V
	I_{rms}	2×7.3A 2×15.9A	2×6.5A 2×15.3A
	Soft switching	ZVS ON	ZVS ON
	Turn-off current	2×8.9A 2×31.5A	2×3.5A 2×23.2A
Diodes	V_{pk}	4×183V	4×188V
	I_{av}	4×2.63A	4×2.63A
	di/dt	2×32.5A/μs 2×31.2A/μs	2×4A/μs 2×23A/μs
Input Inductor	Inductance	2×50μH	2×50μH
	I_{rms}	2×15.3A	2×15.3A
Auxiliary Inductor	Inductance	2×6μH	2×6μH
	I_{rms}	2×6.32A	2×6.07A
Auxiliary Capacitor	Capacitance	2×60μF	2×2.7μF
	V_{pk}	2×195V	2×204V
	I_{rms}	2×6.32A	2×6.07A

B. Design of f_r

As mentioned in Section II, due to smaller switch turn-off current and duty loss, the below-resonance operation is chosen, and the resonant frequency f_r can be obtained from (2) and (11) $f_r \geq 40$ kHz.

C. Design of L_r and C_r

In order to satisfy the ZVS condition, L_r is determined from (28) and (29) by $L_r \geq 6$ μH. From (1), C_r is determined by $C_r \leq 2.7$ μF.

In order to perform a comparison of the proposed RPWM method to the PWM method, the converters have been designed according to the aforementioned specifications and the results are listed in Table I. The improvement of the proposed RPWM method compared to PWM method are summarized as follows.

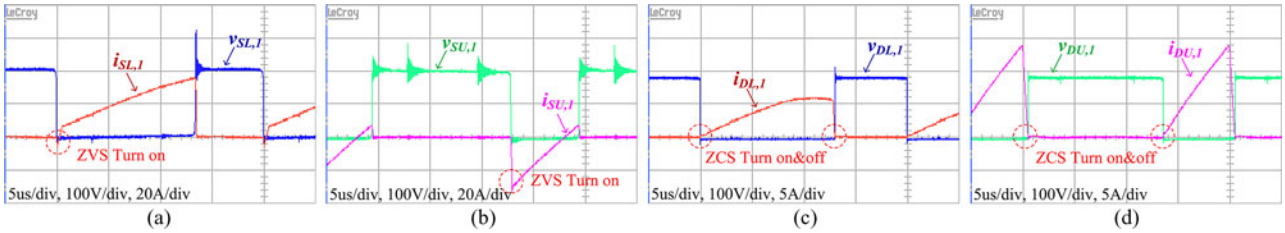

Fig. 11. Experimental waveforms of PWM Method. (a) Voltage and current waveforms of lower switch $S_{L,1}$. (b) Voltage and current waveforms of upper switch $S_{U,1}$. (c) Voltage and current waveforms of lower diode $D_{L,1}$. (d) Voltage and current waveforms of upper diode $D_{U,1}$.

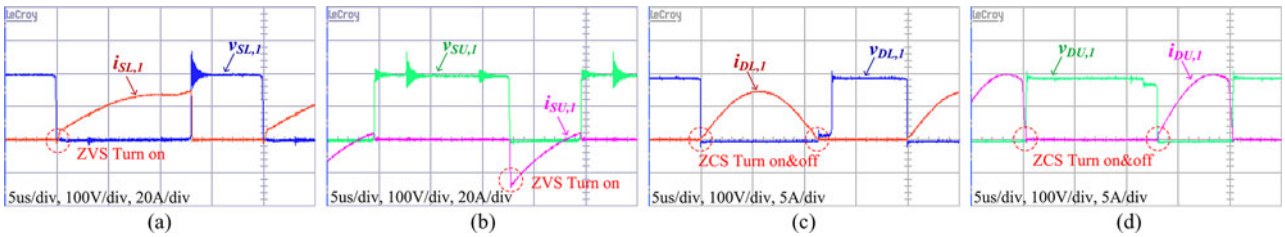

Fig. 12. Experimental waveforms of RPWM Method. (a) Voltage and current waveforms of lower switch $S_{L,1}$. (b) Voltage and current waveforms of upper switch $S_{U,1}$. (c) Voltage and current waveforms of lower diode $D_{L,1}$. (d) Voltage and current waveforms of upper diode $D_{U,1}$.

1) Due to the reduced operating duty, the rms current ratings of the switches are reduced by 5–15%, resulting in reduced conduction losses.
2) Due to the resonant operation, the turn-off current of switches are reduced by 25–60% and falling slopes of the diode current are reduced, resulting in significantly reduced switching losses.
3) The required capacitance of auxiliary capacitor is dramatically reduced to 1/20th, resulting in reduced volume and cost.

IV. Experimental Results

To verify the effectiveness of the proposed converter, a 2-kW prototype of the proposed converter is designed with the specifications used in Section III. Input filter inductor L_f and auxiliary resonant inductor L_r are 50 and 6 μH, respectively. The designed values of auxiliary capacitor $C_{r,1}$ is 2.7 μF 200 V, respectively. An off-the-shelf film capacitor of 2.2 μF 220 V was used for the auxiliary capacitor and a film capacitor of 30 μF 250 V was used for the output capacitor. Both lower and upper switches are implemented with APT75M50B2 (500 V, 75 A, and 75 mΩ) MOSFET. Fast recovery diodes of STTH8R04D (400 V, 8 A, and 25 ns) are used for all rectifier diodes.

Figs. 11 and 12 show the experimental waveforms at full load condition. Fig. 12(a) and (b) shows that both lower switch $S_{L,1}$ and upper switch $S_{U,1}$ are being turned ON with ZVS. Fig. 12(c) and (d) shows that diodes $D_{L,1}$ and $D_{U,1}$ are being turned ON and OFF with ZCS.

The measured efficiency is shown in Fig. 13. The efficiency was measured by YOKOGAWA WT3000. The maximum efficiency of RPWM method is 95.3% at 1400 W load. The maximum efficiency of PWM method is 94.3% at 1200 W load. The efficiency of the proposed RPWM method is approximately 1% higher than that of the PWM method in most of the output power region. The efficiency improvement of the proposed RPWM method would be more significant in higher power converter. Both switch turn-off current and diode di/dt of the PWM method tend to increase as the output power increases. On the other hand, the switch turn-off current of the proposed RPWM method is limited to filter inductor current, and diodes always operate under ZCS condition despite the fact that the output

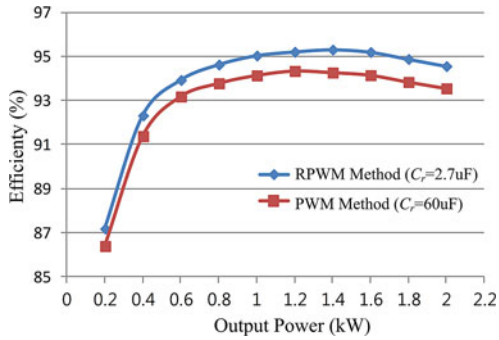

Fig. 13. Comparison of the measured efficiency.

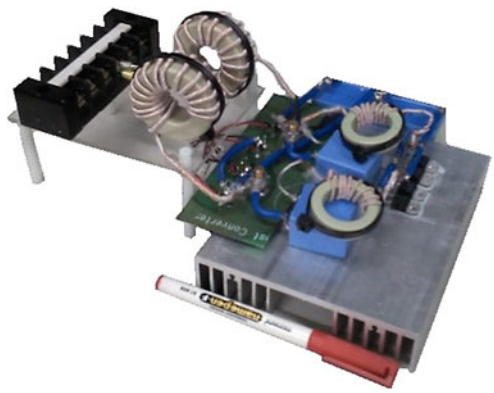

Fig. 14. Photograph of the proposed converter prototype.

power increases. Fig. 14 shows the photograph of the proposed converter.

V. Conclusion

In this paper, an RPWM switching method has been proposed for the high step-up soft-switching dc–dc converter. The following improvements over the PWM method have been achieved: 1) The turn-off losses of the switch are significantly reduced due to reduced turn-off current. 2) The auxiliary capacitor is reduced by 20-fold. 3) The switching losses associated with diode-reverse recovery become negligible even in the small duty cycle. 4) The duty cycle loss is much reduced resulting in increased step-up ratio. Experimental results from a 2-kW prototype demonstrated approximately 1% efficiency improvement of the proposed switching method.

References

[1] K. Hirachi, M. Yamanaka, K. Kajiyama, and S. Isokane, "Circuit configuration of bidirectional DC/DC converter specific for small scale load leveling system," in *Proc. IEE Power Convers. Conf.*, Apr. 2002, vol. 2, pp. 603–609.

[2] Q. Zhao and F. C. Lee, "High-efficiency, high step-up DC–DC converters," *IEEE Trans. Power Electron.*, vol. 18, no. 1, pp. 65–73, Jan. 2003.

[3] T. J. Liang and K. C. Tseng, "Analysis of integrated boost-flyback step-up converter," *Proc. IEE Electr. Power Appl.*, vol. 152, no. 2, pp. 217–225, Mar. 2005.

[4] R. J. Wai and R. Y. Duan, "High-efficiency DC/DC converter with high voltage gain," *Proc. IEE Electr. Power Appl.*, vol. 152, no. 4, pp. 793–802, Jul. 2005.

[5] B. Axelrod, Y. Berkovich, and A. Ioinovici, "Switched coupled-inductor cell for DC-DC converters with very large conversion ratio," in *Proc. IEEE 32nd Annu. Ind. Electron. Conf.*, Nov. 2006, pp. 2366–2371.

[6] M. S. Makowski, "Realizability conditions and bounds on synthesis of switched-capacitor dc–dc voltage multiplier circuits," *IEEE Trans. Circuits Syst. I. Fundam. Theory Appl.*, vol. 44, no. 8, pp. 684–691, Aug. 1997.

[7] O. C. Mak, Y. C. Wong, and A. Ioinovici, "Step-up DC power supply based on a switched-capacitor circuit," *IEEE Trans. Ind. Electron.*, vol. 42, no. 1, pp. 90–97, Feb. 1995.

[8] F. L. Luo and H. Ye, "Positive output multiple-lift push-pull switched-capacitor Luo-converters," *IEEE Trans. Ind. Electron.*, vol. 51, no. 3, pp. 594–602, Jun. 2004.

[9] F. H. Khan and L. M. Tolbert, "A multilevel modular capacitor-clamped DC–DC converter," *IEEE Trans. Ind. Appl*, vol. 43, no. 6, pp. 1628–1638, Nov./Dec. 2007.

[10] D. Cao and F. Z. Peng, "Multiphase multilevel modular DC–DC converter for high-current high-gain TEG application," *IEEE Trans. Ind. Appl.*, vol. 47, no. 3, pp. 1400–1408, May/Jun. 2011.

[11] W. Li and X. He, "High step-up soft switching interleaved boost converters with cross-winding-coupled inductors and reduced auxiliary switch number," *IET Power Electron.*, vol. 2, no. 2, pp. 125–133, Mar. 2009.

[12] W. Li, Y. Deng, R. Xie, J. Shi, and X. He, "Interleaved ZVT boost converters with winding-coupled inductors and built-in LC low pass output filter suitable for distributed fuel cell generation system," in *Proc. IEEE Power Electron. Spec. Conf.*, Jun. 2007, pp. 697–701.

[13] M. Prudente, L. L. Pfitscher, G. Emmendoerfer, E. F. Romaneli, and R. Gules, "Voltage multiplier cells applied to non-isolated DC–DC converters," *IEEE Trans. Power Electron.*, vol. 23, no. 2, pp. 871–887, Mar. 2008.

[14] S. Park and S. Choi, "Soft-switched CCM boost converters with high voltage gain for high-power applications," *IEEE Trans. Power Electron.*, vol. 25, no. 5, pp. 1211–1217, May 2010.

[15] S. Park, Y. Park, S. Choi, W. Choi, and K. Lee, "Soft-switched interleaved boost converters for high step-up and high power applications," *IEEE Trans. Power Electron.*, vol. 26, no. 10, pp. 2906–2914, Oct. 2011.

[16] C. Kim, S. Han, K. Park, and G. Moon, "A new high efficiency ZVZCS bidirectional DC/DC converter for HEV 42 V power systems," *J. Power Electron.*, vol. 6, no. 3, pp. 271–278, Jul. 2006.

[17] J. Kim, D. Jung, S. Park, C. Won, Y. Jung, and S. Lee, "High efficiency soft–switching boost converter using a single switch," *J. Power Electron.*, vol. 9, no. 6, pp. 929–939, Nov. 2009.

[18] H. Do, "Zero–voltage–switching boost converter using a coupled inductor," *J. Power Electron.*, vol. 11, no. 1, pp. 16–20, Jan. 2011.

Yohan Park was born in Seoul, Korea, in 1980. He received the B.S. and M.S. degrees from the Department of Control and Instrumentation Engineering, Seoul National University of Science and Technology (Seoul Tech), Seoul, Korea, in 2009 and 2011, respectively.

He is currently an Engineer with the Electric Vehicle Component Research and Development Group, LG Electronics Company, Seoul, Korea. His research interests include battery charger for electric vehicle and dc–dc converter for renewable energy.

Byoungkil Jung was born in Seoul, Korea, in 1985. He received the B.S. degree from the Department of Control and Instrumentation Engineering, Seoul National University of Science and Technology (Seoul Tech), Seoul, Korea, in 2011, where he is currently working toward the M.S. degree.

His research interests include resonant bidirectional dc–dc converter and dc–dc converter for electric vehicle.

Sewan Choi (S'92–M'96–SM'04) received the B.S. degree in electronic engineering from Inha University, Incheon, Korea, in 1985, and the M.S. and Ph.D. degrees in electrical engineering from Texas A&M University, College Station, in 1992 and 1995, respectively.

From 1985 to 1990, he was a Research Engineer with Daewoo Heavy Industries. From 1996 to 1997, he was a Principal Research Engineer at Samsung Electro-Mechanics Company, Korea. In 1997, he joined the Department of Control and Instrumentation Engineering, Seoul National University of Science and Technology (Seoul Tech), Seoul, Korea, where he is currently a Professor. His research interests include power conversion technologies for renewable energy systems and energy storage systems and dc–dc converters and battery chargers for electric vehicles.

Dr. Choi is an Associate Editor of the IEEE Transactions on Power Electronics and IEEE Transactions on Industry Applications.